ACS APPLIED MATERIALS & INTERFACES

Research Article

www.acsami.org

Mechanical Ball-Milling Preparation of Fullerene/Cobalt Core/Shell Nanocomposites with High Electrochemical Hydrogen Storage Ability

Di Bao,[†] Peng Gao,*[,†] Xiande Shen,[†] Cheng Chang,[†] Longqiang Wang,[†] Ying Wang,[†] Yujin Chen,*[,‡] Xiaoming Zhou,[†] Shuchao Sun,[†] Guobao Li,[§] and Piaoping Yang*[,†]

[†]Micro & Nano Material Research Institute, College of Materials Science and Chemical Engineering, and [‡]College of ScienceHarbin Engineering University, Harbin, Heilongjiang 150001, P. R. China

[§]Beijing National Laboratory for Molecular Sciences, State Key Laboratory of Rare Earth Materials Chemistry and Applications, Peking University, Beijing 100871, P. R. China

ABSTRACT: The design and synthesis of new hydrogen storage nanomaterials with high capacity at low cost is extremely desirable but remains challenging for today's development of hydrogen economy. Because of the special honeycomb structures and excellent physical and chemical characters, fullerenes have been extensively considered as ideal materials for hydrogen storage materials. To take the most advantage of its distinctive symmetrical carbon cage structure, we have uniformly coated C_{60}'s surface with metal cobalt in nanoscale to form a core/shell structure through a simple ball-milling process in this work. The X-ray diffraction (XRD), scanning electron microscope (SEM), Raman spectra, high-solution transmission electron microscopy (HRTEM), energy-dispersive X-ray spectrometry (EDX) elemental mappings, and X-ray photoelectron spectroscopy (XPS) measurements have been conducted to evaluate the size and the composition of the composites. In addition, the blue shift of C_{60} pentagonal pinch mode demonstrates the formation of Co−C chemical bond, and which enhances the stability of the as-obtained nanocomposites. And their electrochemical experimental results demonstrate that the as-obtained C_{60}/Co composites have excellent electrochemical hydrogen storage cycle reversibility and considerably high hydrogen storage capacities of 907 mAh/g (3.32 wt % hydrogen) under room temperature and ambient pressure, which is very close to the theoretical hydrogen storage capacities of individual metal Co (3.33 wt % hydrogen). Furthermore, their hydrogen storage processes and the mechanism have also been investigated, in which the quasi-reversible C_{60}/Co↔C_{60}/Co−H_x reaction is the dominant cycle process.

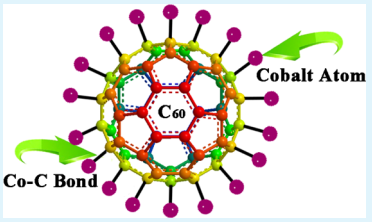

KEYWORDS: *C_{60}/Co, ball-milling, core/shell, Co−C bond, nanocomposite, electrochemical hydrogen storage*

INTRODUCTION

Hydrogen, which is a renewable resource and free of pollution, is a very promising resource for the application in powered vehicles. However, the major impediment is that it is difficult to be high-capacity stored within an effective, safe, and stable solid-state medium, which restricts its practical application. Nowadays, effective hydrogen storage has been regarded as a key technology for realizing the hydrogen economy and considered as one of the highest technical priorities.[1] Although the storage of liquid hydrogen in cryogenic containers enables better volume efficiency, about 1/3 of the stored energy has to be used for liquefaction and hydrogen will be lost due to evaporation.[2] Therefore, with a future perspective, solid-state hydrogen storage materials are more likely to meet the requirements: appropriate thermodynamics, fast kinetics, high storage capacity, effective heat transfer, lightweight, long cycle life, and safety. Up to now, many storage medium have been developed to uptake as much as hydrogen storage, such as metal alloys, boron nitride, metal−organic frameworks.[3−7]

Recently, a series of Co-based materials are reported to have high reversible discharge capacity and good cycle life as negative electrode materials of electrochemical hydrogen storage cells, and their electrochemical hydrogen storage capacities are obviously improved after mixing some non-metallic materials such as Si, B, P, S, BN, and so on.[8−13] Moreover, it is found that the nonmetallic material can improve the dispersion and increase the contact area between alkaline solution and active materials.[14] In addition, carbon/cobalt materials, such as graphene/Co and CNTs/Co, have showed excellent electrochemical performances.[15] Compared with the nonmetallic materials mentioned above, carbon can not only improve the dispersion of materials, but also increase their electroconductibility.[16] However, the low level hydrogen storage ability of single carbon materials at standard temperature and pressure is far from satisfactory,[17,18] which is mainly due to its rapid escape from the space between carbon skeleton construction[19] and the absorption to the exterior of the carbon layer via van der Waals interactions needing a large binding energy to keep steady.[20−22]

Received: November 29, 2013
Accepted: February 5, 2014
Published: February 5, 2014

Fullerenes (C_{60}), owning a distinctive symmetrical carbon cage structure, has become the object of intensive research since their discovery thirty years ago. Compared with other carbon materials, C_{60} has higher surface area and may be a better matrix material for functional composite materials. Recently it has been paid an attention by researchers through the theoretical computation via carbon−carbon double bonds with hydrogen that C_{60} has a high gaseous hydrogen storage capacity (7.70 wt % hydrogen).[23] However, our practical measurement of the C_{60} hydrogen storage demonstrates that the capacity of individual C_{60} is very low at room temperature under ambient pressure, as shown in Table 1. Considering the improved hydrogen storage abilities through the composition of carbon/cobalt materials mentioned above, C_{60}/Co core−shell composite is predicted as a hydrogen storage material with high capacity.

Table 1. Test Conditions and Electrochemical Hydrogen Store Capacities of Co, C_{60} and C_{60}/Co

materials	test condition	hydrogen storage capacity (wt % hydrogen)
Co[30]	298 K and 101 KPa	3.3 (theoretical computation)
Co nanocrystalline[31]	298 K and 101 KPa	1.58
C_{60}[23]	823−873 K and 101KPa	7.70 (theoretical computation)
C_{60} (this work)	298 K and 101 KPa	0.69
C_{60}/Co (this work)	298K and 101KPa	3.32

Recently, C_{60}/Co nanocomposites have been prepared through physical codeposition or metal ion implantation methods.[24,25] In order to achieve the desired stable C_{60}/Co composites depending on the formation of Co−C chemical bond, high temperature and high pressure in the experiments are required.[24−27] In the past, mechanical ball-milling method has been proved as an effective physical-chemical mean to obtain metal/carbon compounds.[15,28] In this paper, we obtain the C_{60}/Co core/shell nanocomposites through a simple ball-milling method using raw materials of Co and C_{60} as the precursors. Furthermore, comparing with the pure C_{60} Raman spectrogram, we observe a blue shift of pentagonal pinch mode, which is caused by the charge transfer from surrounding Co atoms to fullerene molecule.[29] The formation of Co−C chemical bond enhances the stability of their structures and the cycle reversibility is better than other previous graphene/Co composites. The as-obtained product display a much larger electrochemical hydrogen storage capacity of 3.32 wt % hydrogen, which is ∼2.10 times of the result for chemical precipitation prepared Co nanoparticles and close to the theoretical hydrogen storage capacities of individual metal Co, as shown in Table 1. In addition, their hydrogen storage processes and the mechanism have been proved as a quasi-reversible C_{60}/Co ↔ C_{60}/Co−H_x reaction for the dominant cycle process. Additionally, the mechanical ball-milling method, optimizing the predominant electrochemical hydrogen storage performance of the metal−fullerene nanocomposites, inspirits us to develop it. This research work may also open the window to other fullerene/transition metal nanocomposites for hydrogen storage.

EXPERIMENTAL SECTION

C_{60} used in this work were purchased from Puyang Yongxin Fullerene Technology Co., Ltd., and their purity specification is 99.9%. In a

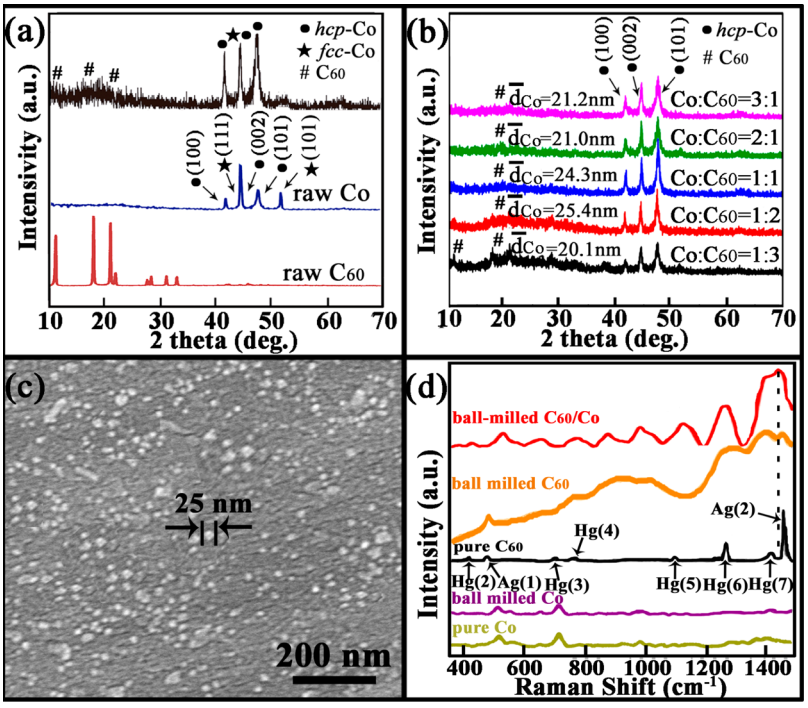

Figure 1. (a) XRD patterns of raw Co, C_{60}, and the ball-milled composite obtained at a balling-speed of 200 r/min with the precursors of m_{Co}:m_{C60} = 1:1 for 10 h under an Ar gas atmosphere; (b) XRD patterns of the ball-milled composites obtained at a balling-speed of 400 r/min for 10 h with different Co to C_{60} weight ratio under Ar gas atmosphere; (c) SEM image of the ball-milled C_{60}/Co composite with m_{Co}:m_{C60} = 1:1 obtained at a balling-speed of 400 r/min for 10h; (d) Raman spectra of the as-obtained C_{60}/Co composite with m_{Co}:m_{C60} = 1:1 at a balling-speed of 400 r/min for 10 h, pure raw materials (Co and C_{60}) before and after ball milling at a speed of 400 r/min for 10 h.

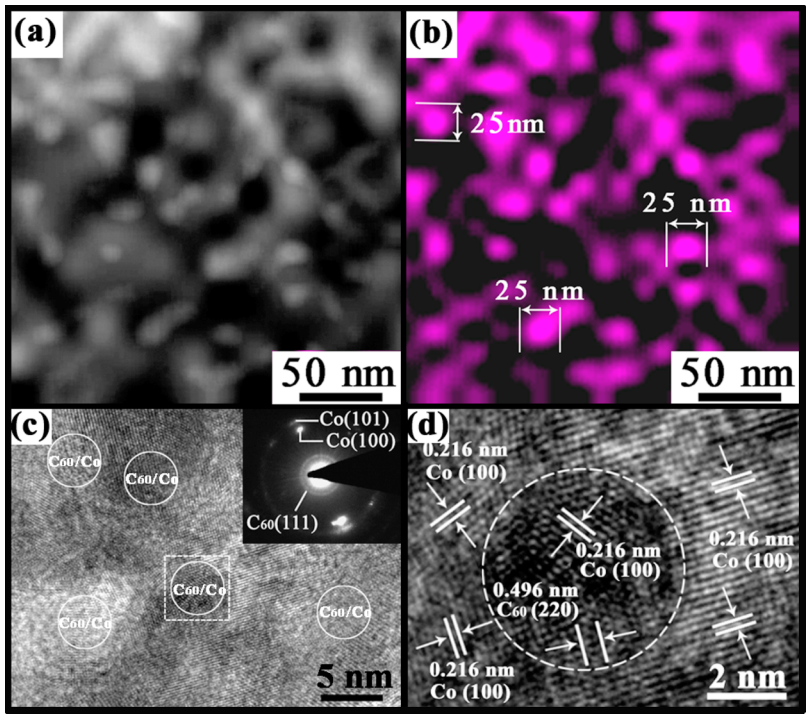

Figure 2. (a) ADF-STEM image of C_{60}/Co composite; (b) corresponding EDX elemental mappings of Co element; (c) HRTEM image of the obtained C_{60}/Co composites, the circle area is C_{60} concentration zone; inset, the corresponding SAED pattern of the rectangular area; (d) C_{60}/Co composites enlarged from the rectangular area, showing the core/shell structure of C_{60}/Co.

typical experiment, Co powders (purity 99.9%, 200 mesh, Shanghai Xingzhi chemical factory) were first blended together (the Co to C_{60} weight ratio was 0.3−3:1). All samples were ball-milled using a planetary ball mill (pulverizette 7, FRITSCH) in a stainless steel vessel at the speed of 400 rounds per minute for 10 h under Ar gas atmosphere. The tungsten carbide balls of 2 mm diameter were employed as ball-milling medium. The ball-to-powder weight ratio was 15:1. After cooling to room temperature, the obtained powders were collected. All the samples were characterized by X-ray diffraction (Rigaku D/max IIIA, Cu Kα). The scan rate of 0.05°/s was used to record the patterns in the 2θ range of 10−70°. Raman spectroscopic analysis was performed by using a micro-Raman system with an Ar ion laser 488 nm, and a probing laser 50 W/cm^2 was guided during the illumination. Field-emission scanning electron microscopy (FESEM) images were obtained by a SU8000 cold emission field scanning electron microanalyser (Hitachi, Japan), whereby the resulting powders were mounted on a copper slice. High resolution transmission electron microscopy (HRTEM) and scanning transmission electron microscopy (STEM) images were recorded on a JEOL-2010 TEM at an acceleration voltage of 200 KV. X-ray photoelectron spectroscopy (XPS) was performed by using a PHI 5700 ESCA System with a monochromatic Al Kα (1486.6 eV) radiation source and a hemisphere detector. The electrochemical charge and discharge curves were measured in a two-electrode test cell by a LAND battery-test instrument (CT2001A), which contained one piece of positive electrode and one piece of negative electrode. The negative electrode was made of 85 wt % C_{60}/Co powder, 10 wt % acetylene black. The positive electrode material consisted of 80 wt % nickel hydroxide, 15 wt % Co. Each of the positive and negative electrode material was mixed with 5 wt % PTFE to form a paste, and coated on a 1 cm^2 Ni-foam. The electrolyte was 6 M KOH aqueous solution. The electrode plate was pressed at a pressure of 50 kg/cm^2 for 30 s. The negative electrodes were charged at a current density of 100 mAh/g for 8 h, and then discharged to 0 V at a current density of 30 mAh/g. In order to study the rate capability of C_{60}/Co composites, the negative electrodes were charged at a current density of 100 mAh/g for 8 h, and then discharged to 0 V at current density of 200−1000 mAh/g. The cyclic voltammetry (CV) and electrochemical impedance spectroscopy (EIS) were conducted by using an electrochemical workstation (CHI660D) of three-electrode test cell. The cell consisted of C_{60}/Co as the working electrode, a metal platinum gauze as the counter electrode and a Ag/AgCl electrode as the reference electrode, and the electrolyte was 6 M KOH. The scan range was between −1.2 and 0 V vs Ag/AgCl, and the scan started from the open circuit potential and then along the negative direction at a scan rate of 10 mV/s. All the experiments were conducted at room temperature.

RESULTS AND DISCUSSION

Structure, Morphology, Composition, and Formation Mechanism of C_{60}/Co Nanocomposite. First, the overall phase, crystallinity and purity of the raw materials and the as-synthesized samples were examined by XRD measurements. As shown in Figure 1a, the original Co powders have two phases: fcc phase (PCPDF89−4307) and hcp phase (PCPDF89−4308). And the XRD pattern of C_{60} with strong diffraction peaks is attributed to its fcc phase (PCPDF79−1715), which demonstrates that C_{60} is well-crystallized and without the impurities. It is also found that when the ball-milling speed is 200 r/min, the products' XRD results are similar to the combination of raw materials' spectrum, which maybe due to the deficient grain refinement and the weak composite structures under a lower activation energy induced by a lower speed ball-milling. Considering the reaction of metal Co with carbon materials for Co_3C compound when the ball-milling speed nears 500 r/min,[15] a suitable ball-milling speed (400 r/min) is selected in this work. After ball-milling the raw materials under Ar atmosphere for some hours, it was found that all diffraction peaks corresponding to Co were broadened, as shown in Figure 1a, which indicates that the Co crystalline grains were refined. In addition, the phase transformation of fcc-cobalt into hcp-cobalt has also been observed. As reported, that lattice surface energy of fcc-Co (~2.05 × 10^{-18} J/unit lattice) is lower than that of hcp-Co (2.61 × 10^{-18} J/unit

dx.doi.org/10.1021/am405458u | ACS Appl. Mater. Interfaces 2014, 6, 2902−2909

lattice), and hcp-Co is a more stable phase.[32] Here we indicate that the sample's average crystallization size of metal Co is 20−25 nm calculated by the Scherrer equation from the XRD pattern in Figure 1b, which implies the efficient refinement process in this work.

Figure 1c shows the typical SEM image of the as-prepared C_{60}/Co composite after ball-milling for 10 h at 400 r/min. It can be seen that the as-prepared products contain regular tiny nanospherical morphology, and the size of nanoparticles is ∼25 nm. Their good combination effect through the ball-milling process is further confirmed by the Raman analysis, which is conducted by using a micro-Raman spectrometer with an Ar ion laser (488 nm^{-1}). As shown in Figure 1d, the peak positions of pure cobalt and C_{60}'s Raman spectra have not changed under the high speed ball-milling conditions at 400r for 10h. And the Raman spectrum of pure C_{60} shows the pronounced peaks assigned to its Raman-active modes with the icosahedral symmetry, namely the nondegenerate Ag(n) modes and the degenerate Hg(n) modes.[33] In the Raman spectrum of the C_{60}/Co composite, the increased number of peaks, and the additional peaks are attributed to a series of the Raman-forbidden modes and the split components of the Raman-active modes by the symmetry lowering of C_{60}, which are due to the formation of the C_{60}/Co composite.[34−37] Taking account of the energy differences between the respective modes and the overlapped features in the broad peaks, it can be remarked that the most series of the C_{60} I_h– modes are observed including the IR-active F_u modes (e.g., peak for the expansion or contraction vibration at 884, 992 cm^{-1} and peaks for twisting vibration of the C_{60} clusters at 1272 cm^{-1} based on orthogonal tight-binding molecular dynamic simulations),[34−36] which become Raman-active by the loss of inversion symmetry of C_{60}. Moreover, the careful analysis of pentagonal pinch mode Ag(2) in terms of the peak position at 1460 cm^{-1} of pure C_{60} provides the information on the changes occurred in the as-obtained C_{60}/Co composite. Comparing with the pure C_{60} Raman spectrogram, the C_{60}/Co shows a blue shifting and broadening in Ag(2) pentagonal pinch mode, which is caused by the charge transfer from surrounding Co atoms to fullerene molecule,[38] which should be due to the formation of C−Co bond. The downshift of Ag(2) mode in this work also proves the theoretical calculations on Raman evaluation of the metal-fullerene systems, which is predicted by Dresselhaus et al.[39] As is reported,[24,40] C_{60}/Co nanocomposites were produced through physical codeposition process, which displayed very weak Co−C bond. In contrast, the C_{60}/Co composite obtained here by high-energy ball-milling exhibits strong structure stability. So it is reasonable to believe that the high activation energy coming from the mill balls crashing makes metal cobalt react with carbon atoms of C_{60} and Co is tightly banded on the C_{60} skeleton.

More details about the composite structures of the product are further investigated through TEM measurements. Figure 2a is an annular dark-field (ADF) scanning transmission electron microscopy (STEM) image of the C_{60}/Co composite, and Figure 2b is the corresponding energy dispersive X-ray spectrometry (EDX) elemental mappings of Co elements. As shown in Figure 2b, particle size is about 25 nm, which is in good agreement with the above SEM results. The HRTEM image of C_{60}/Co composite confirms that the nanoparticles contain many dark/light stripes, which are further distinguished by circles in Figure 2c. To achieve more precise information, we provide a magnified image of a distinct segment in Figure 2d. The HRTEM image of the sample clearly reveals lattice spacing of 0.216 nm corresponding to the (100) plane of hcp-Co in outer circle. However, the angles of Co in HRTEM image are inconsistent with Steno's law of constant angles,[41] which proves the existence of muliti-layered Co and further confirms the formation process of the Co shell through a layer-by-layer steps, which should be a Kossel Stranski nucleation process.[42] The lattice spacing of 0.496 nm is clearly observed in inner circles, which is related to the (220) plane of fcc-C_{60}. As the surface of C_{60} molecules have been closely coated by Co, Co (100) plane is also observed in circles. Moreover, the sample's composition and crystallization are further confirmed by its SAED result. As shown in Figure 2c inset, the reflections from the Co and C_{60} are observed, in which the appearance of the diffraction rings and spots indicates the polycrystalline nature of the nano-composite.

The composition of the C_{60}/Co composite is further analyzed by XPS measurement. As shown in Figure 3a, the survey spectrum exhibits a strong Co signal, some C signal and small signal of O element, which confirms the element composition of the product. Figure 3b displays the Co 2p spectrum of the as-prepared products, in which there are two peaks at binding energies of 779.2 and 795.6 eV, respectively. Both the peaks are assigned to metallic cobalt.[43,44] Figure 3c shows the product's C 1s spectrum. In the spectrum, there is an obvious peak at 284.6 eV and C 1s shakeup satellite peaks in 280−294 eV range, which originates from the sp^2-hybridized carbon bond of fullerene.[45,46] In addition, a broaden peak at 285.2 eV is found, which is attributed to the sp^3-hybridized carbon bond[47−49] and further demonstrates the formation of C−Co bond.

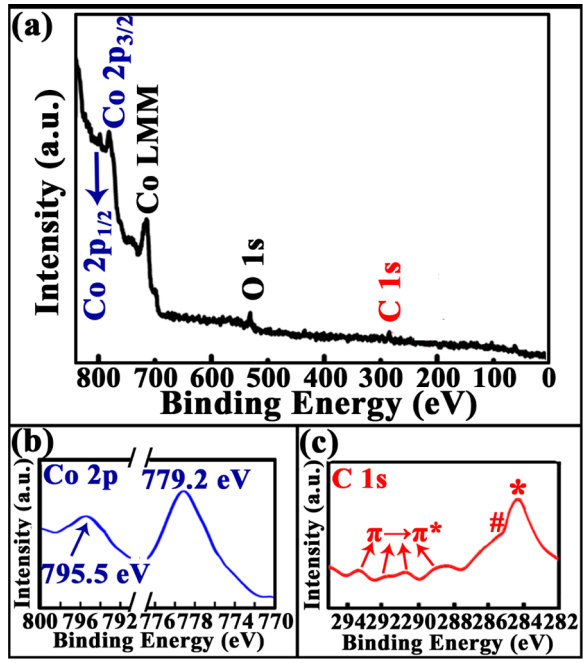

Figure 3. (a) XPS spectrum of the as-obtained C_{60}/Co composite; (b) Co 2p spectrum; (c) C 1s spectrum, the shakeup satellite peaks are attributed to C_{60} extended aromatic systems, the # peak at 285.2 eV is assigned to sp^3-hybridized carbon bond; the * peak at 284.6 eV is assigned to sp^2-hybridized carbon bond.

On the basis of the above results and analysis, the formation process of C_{60}/Co nanostructures is clearly shown in Scheme 1.

Scheme 1. Illustration of the Formation Process of C_{60}/Co Core/Shell Composites

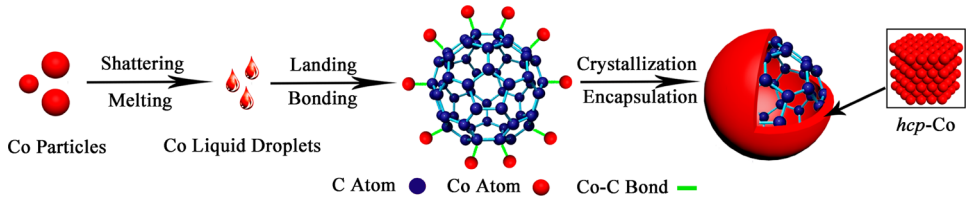

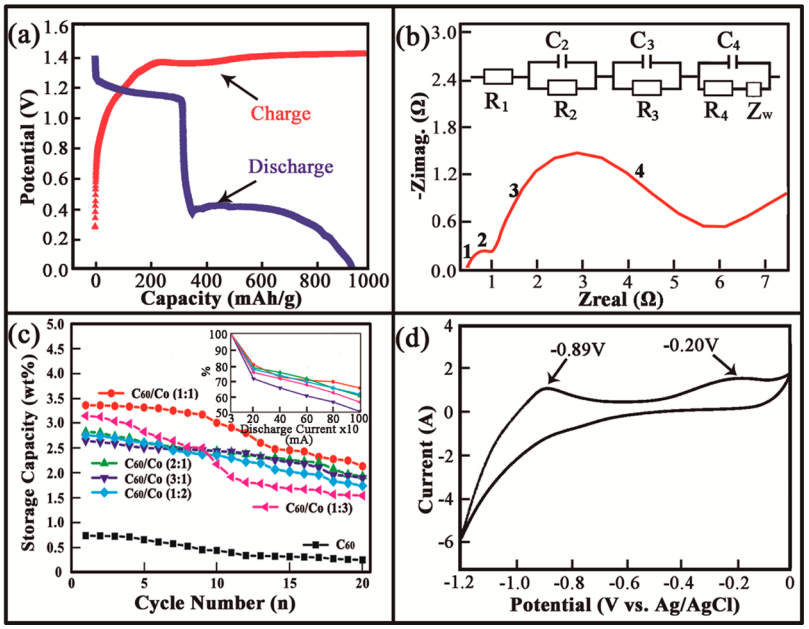

Figure 4. (a) Charge−discharge curves of the C_{60}/Co composites (m_{C60}:m_{Co} = 1:1); (b) electrochemical impedance spectroscopy (EIS) of the C_{60}/Co composites electrode at 6 M KOH solution, the inset is equivalent circuit used for simulating the impedance spectra of the C_{60}/Co composites electrode; (c) cycle performances of pure C_{60} and as-obtained C_{60}/Co composites, the inset is retention rate of C_{60}/Co composite electrodes at various discharge current densities to the discharge current density of 30 mA; (d) cyclic voltammogram curve of the C_{60}/Co composite (m_{Co}:m_{C60} = 1: 1) vs Ag/AgCl in 6 M KOH solution.

First, under the high speed ball-milling conditions, the bulky Co precursor is shattered by the crashing of the tungsten carbide milling balls and melts. Second, the Co liquid droplets freely land on the surface of C_{60} and Co−C bond forms. Because of the good thermal conductivity and bearing capacity of C_{60}, the liquid Co quickly recrystallizes on C_{60} matrixes and the C_{60}/Co composite forms.

Electrochemical Hydrogen Storage Properties. To further investigate the hydrogen storage ability of the C_{60}/Co composites, the electrochemical hydrogen storage cycles of the C_{60}/Co electrode at a discharge current density of 30 mA/g is first tested, as shown in Figure 4a. In the charge process, one charge plateau appears at about 1.40 V, which can be attributed to the reaction of C_{60}/Co → C_{60}/Co−H_x.[10,50] In the discharge curve, two obvious plateaus are observed at 1.17 and 0.43 V, respectively, which suggests that different hydrogen desorption sites exist in the C_{60}/Co nanocomposite. The discharge plateaus appearing at about 0.43 V should be attributed to the desorption of hydrogen adsorbed on the surface of the nanocomposite.[13,51] The discharge plateau appearing at about 1.17 V is comparable to those of other Co based alloys,[52] which is due to the reaction of C_{60}/Co−H_x → C_{60}/Co. It is also noted that the suitable length of both the charge and discharge plateaus indicate the excellent reversibility and Coulombic efficiency of the electrode. Figure 4b illustrates the electrochemical impedance spectroscopy (EIS) of the composite electrode. The spectrum consists of a smaller semicircle in the high-frequency region and a larger semicircle in the low-frequency region followed by a straight line. It is pointed out that the measured high-frequency semicircle is the contact resistance between the current collector and the composites, and the lower frequency semicircle is the charge-transfer reaction resistance.[53] Furthermore, the EIS data is fitted using an equivalent circuit in Figure 4b The capacitive components labeled by C are modeled as constant-phase elements (CPE) to describe the depressed nature of the semicircles. R_1 (0.418 Ω) is ascribed to the electrolyte resistance between the electrode and the reference electrode. The semicircle in the high-frequency region, modeled by R_2 (2.816Ω) and C_2 (0.376F), comes from the contact resistance between the C_{60}/Co composites and the current collector. The contact resistance and capacitance between the C_{60}/Co generate the parameters of R_3 (0.340 Ω) and C_3 (7.015×10^{-3}F), respectively. R_4 (4.802 Ω) and C_4 (1.035 F), representing the semicircle in the low-frequency region, contribute to the charge-transfer reaction resistance and the double-layer capacitance, respectively, and Z_w (1.716 Ω) is the Warburg impedance. Through comparing the resistance values, the charge-transfer reaction should be the main reaction process.

Furthermore, the cycle performances demonstrate that the as-prepared C_{60}/Co composites own satisfactory stability as electrochemical hydrogen storage materials. Figure 4c shows

the discharge capacities and the cycle stability of C_{60}/Co composites and pure C_{60} electrodes at a discharge current density of 30 mA/g. It is clear that the pure C_{60} powders' low capacity is 189 mAh/g (0.69 wt % hydrogen), which is attributed to hydrogen's rapid escaping from the space between its unclosed cage frameworks. After wrapped by metal Co, the discharge capacities of the C_{60}/Co composites increase to a certain degree. In particular, the C_{60}/Co composite (m_{C60}:m_{Co} = 1: 1) electrode can achieve a maximum discharge capacity as high as 907 mA h/g (3.32 wt % hydrogen), which is ~2.10 times of the result for chemical precipitation prepared Co nanoparticles[31] and close to the theoretical hydrogen storage capacities of individual metal Co.[30] Even after 20 cycles, the discharge capacity still remains at 575 mAh/g (2.10 wt % hydrogen). Compared with traditional AB_5[54,55] type, AB_2[56] type, AB type,[57] and Mg-based alloy[58−60] hydrogen storage materials, the as-prepared C_{60}/Co composites display a much higher discharge capacity and cycling stability, which are due to their good composite structure.

Just as we have known, highly dispersed C_{60} hinders the aggregation of Co and increases the special surface of the nanocomposites, which contributes to a larger efficient surface area with hydrogen.[52] Another important reason is that the C_{60} frameworks can reduce the internal resistance and maintain the good cycle performance of the electrode. Besides the above two reasons, the interesting core/shell structured C_{60}/Co composites also contributes to the high hydrogen storage capacity. In this paper, metal cobalt has been tightly pressed on fullerene through the ball-milling process, which results in the steady formation of C_{60}/Co nanocomposites. Therefore, the structure relaxation effect coming from the hydrogen adsorption−desorption process would be withstood. The stable C_{60}/Co nanocomposites also exhibit good electrochemical hydrogen storage performances at high current densities. To investigate the kinetic characteristics of the C_{60}/Co composites electrodes, the rate capability is measured at different current densities. The inset in Figure 4c shows the cycling performances of the nanocomposites at larger discharge current densities. When the current density changes from 30 to 1000 mA, the discharging capacity of mass ratio 1:1 varies from 907 to 589 mAh/g at the first cycle of all the composites. The discharge capacities of all the composites at different current densities are summarized in Table 2. As shown in table 2, even at a high current density of 1000 mAh/g, the lowest hydrogen storage capacity of the C_{60}/Co composite (the mass rate is 3:1) is much higher than that of single C_{60} or Co.

Finally, cyclic voltammogram curve (CV) is carried out to further investigate the electrochemical hydrogen adsorption−desorption behaviors of C_{60}/Co nanocomposites as shown in Figure 4d. The main CV feature of the sample shows two pairs of remarkable cathodic and anodic current peaks, which is different from the previous reports only exhibit one pair of peak.[61] In the reversed scan, two strong oxidation peaks center at −0.89 and −0.20 V that are far from the equilibrium potentials of pure Co and C_{60}.[9,62] The potential position and feature of the anodic peak at −0.89 V agree with the electrochemical oxidation of hydrogen in crystal lattice, as reported in literature.[10,24,28] The current peak appearing at about −0.20 V may be the electrochemical oxidation of hydrogen adsorbed on the surface of the electrode material, which are frequently observed for the electrochemical hydrogen storage electrodes.[33,63] Moreover, the cathodic peak is attributed to the hydrogen adsorption on the composite's electrode.[10] Thus, the redox peaks can be attributed to a reversible electrochemical hydrogen adsorption−desorption reaction taking place on the C_{60}/Co electrode. According to earlier results on the electrochemical reaction of Co in hydrogen storage process,[30] the reversible CV peaks observed here are ascribed to the quasi-reversible electrochemical reaction

$$C_{60}/Co + xH_2O + xe^- \leftrightarrow C_{60}/Co - H_x + xOH^-$$

Table 2. Discharge Capacities of All the C_{60}/Co Composites at Current Densities from 30 mA to 1000 mA

	electrochemical hydrogen storage capacity (mAh/g)				
current rates (mA)	1:1[a]	2:1	3:1	1:2	1:3
30	907	763	744	714	849
200	725	595	506	573	698
400	653	572	464	543	661
600	635	542	428	514	624
800	626	496	400	484	577
1000	590	458	357	454	521

[a]The specific value is mass ratio of C_{60} to Co.

CONCLUSIONS

In summary, C_{60}/Co core/shell composites have been successfully prepared via a direct physical-chemical ball-milling method and their electrochemical hydrogen storage properties are studied for the first time. The product exhibits a stable composite structure due to the formation of Co−C bond and has high hydrogen storage capacity and good cycle stability. It is also found that the quasi-reversible reaction C_{60}/Co ↔ C_{60}/Co−H_x is dominant for the electrochemical hydrogen storage process.

AUTHOR INFORMATION

Corresponding Authors

*E-mail: gaopeng@hrbeu.edu.cn.
*E-mail: chenyujin@hrbeu.edu.cn.
*E-mail: yangpiaoping@hrbeu.edu.cn.

Notes

The authors declare no competing financial interest.

ACKNOWLEDGMENTS

We thank the Program for NCET in University (NCET-13-0754); the Natural Science Foundation of China (Grant 51272050 and 51072038); the Specialized Research Fund for the Doctoral Program of Higher Education of China (20092304120021); Harbin Sci-tech innovation foundation (RC2012XK017012); Harbin Key Sci-tech project (2010AA4BG004); the Fundamental Research funds for the Central Universities (HEUCF2014); and Outstanding Youth Foundation of Heilongjiang Province (Grant JC201008) for the financial support of this research.

REFERENCES

(1) Satyapala, S.; Petrovicb, J.; Reada, C.; Thomasc, G.; Ordaza, G. The U.S. Department of Energy's National Hydrogen Storage Project: Progress towards Meeting Hydrogen-powered Vehicle Requirements. *Catal. Today* **2007**, *120*, 246−256.

(2) Rowsell, J. L. C.; Yaghi, O. M. Strategies for Hydrogen Storage in Metal−Organic Frameworks . *Angew. Chem., Int. Ed.* **2005**, *44*, 4670−4679.

(3) Cohen, R. L.; Wernick, J. H. Hydrogen Storage Materials: Properties and Possibilities. *Science* **1981**, *214*, 1081−1087.
(4) Dinc, M.; Dailly, A.; Liu, Y.; Brown, C. M.; Neumann, D. A.; Long, J. R. Hydrogen Storage in a Microporous Metal−Organic Framework with Exposed Mn^{2+} Coordination Sites. *J. Am. Chem. Soc.* **2006**, *128*, 16876−16883.
(5) Latroche, M.; Surblé, S.; Serre, C.; Mellot-Draznieks, C.; Llewellyn, P. L.; Lee, J. H.; Chang, J. S.; Jhung, S. H.; Férey, G. Hydrogen Storage in the Giant-pore Metal−organic Frameworks MIL-100 and MIL-101. *Angew. Chem., Int. Ed.* **2006**, *45*, 8227−8231.
(6) Vitillo, J. G.; Regli, L.; Chavan, S.; Ricchiardi, G.; Spoto, G.; Dietzel, P. D. C.; Bordiga, S.; Zecchiana, A. Role of Exposed Metal Sites in Hydrogen Storage in MOFs. *J. Am. Chem. Soc.* **2008**, *130*, 8386−8389.
(7) Ma, R.; Bando, Y.; Zhu, H.; Sato, T.; Xu, C.; Wu, D. Hydrogen Uptake in Boron Nitride Nanotubes at Room Temperature. *J. Am. Chem. Soc.* **2002**, *124*, 7672−7673.
(8) Wang, Y.; Lee, J. M.; Wang, X. An Investigation of the Origin of the Electrochemical Hydrogen Storage Capacities of the Ball-milled Co-Si Composites. *Int. J. Hydrogen Energy* **2010**, *35*, 1669−1673.
(9) Liu, Y.; Wang, Y. J.; Xiao, L. L.; Song, D. W.; Wang, Y. P.; Jiao, L. F.; Yuan, H. T. Structure and Electrochemical Behaviors of a Series of Co-B Alloys. *Electrochim. Acta* **2008**, *53*, 2265−2271.
(10) Cao, Y. L.; Zhou, W. C.; Li, X. Y.; Ai, X. P.; Gao, X. P.; Yang, H. X. Electrochemical Hydrogen Storage Behaviors of Ultra fine Co-P Particles Prepared by Direct Ball-milling Method. *Electrochim. Acta* **2006**, *51*, 4285−4290.
(11) Song, D. W.; Wang, Q. H.; Wang, Y. P.; Wang, Y. J.; Han, Y.; Li, L.; Liu, G.; Jiao, L. F.; Yuan, H. T. Liquid Phase Chemical Synthesis of Co-S Microspheres with Novel Structure and Their Electrochemical Properties. *J. Power Sources* **2010**, *195*, 7462−7465.
(12) Wang, Q. H.; Jiao, L. F.; Han, Y.; Du, H. M.; Peng, W. X.; Huan, Q. N.; Song, D. W.; Si, Y. C.; Wang, Y. J.; Yuan, H. T. CoS_2 Hollow Spheres: Fabrication and Their Application in lithium-ion Batteries. *J. Phys. Chem. C* **2011**, *115*, 8300−8304.
(13) Lu, Z. W.; Yao, S. M.; Li, G. R.; Yan, T. Y.; Gao, X. P. Microstructure and Electrochemical Properties of the Co-BN Composites. *Electrochim. Acta* **2008**, *53*, 2369−2375.
(14) Song, D. W.; Xu, Y. N.; An, C. H.; Wang, Q. H.; Wang, Y. P.; Li, L.; Wang, Y. J.; Jiao, L. F.; Yuan, H. T. Recovered $LiCoO_2$ as Anode Materials for Ni/Co Power Batteries. *Phys. Chem. Chem. Phys.* **2012**, *14*, 71−75.
(15) Yang, S. Q.; Gao, P.; Bao, D.; Chen, Y. J.; Wang, L. Q.; Yang, P. P.; Li, G. B.; Sun, Y. Z. Mechanical Ball-milling Preparation of Mass Sandwich-like Cobalt-graphene Nanocomposites with High Electrochemical Hydrogen Storage Ability. *J. Mater. Chem. A* **2013**, *1*, 6731−6735.
(16) Chang, K.; Chen, W. X. Single-layer MoS_2/Graphene Dispersed in Amorphous Carbon: towards High Electrochemical Performances in Rechargeable Lithium Ion Batteries. *J. Mater. Chem.* **2011**, *21*, 17175−17184.
(17) Dillon, A. C.; Heben, M. J. Hydrogen Storage Using Carbon Adsorbents: Past, Present and Future. *Appl. Phys. A* **2001**, *72*, 133−142.
(18) Züttela, A.; Sudana, P.; Maurona, P.; Kiyobayashib, T.; Emmeneggera, C. Hydrogen storage in carbon nanostructures. *Int. J. Hydrogen Energy* **2002**, *27*, 203−212.
(19) Yürüma, Y.; Taralpa, A.; Veziroglub, T. N. Storage of Hydrogen in Nanostructured Carbon Materials. *Int. J. Hydrogen Energy* **2009**, *34*, 3784−3798.
(20) Yidirim, T.; Ciraci, S. Titanium-decorated Carbon Nanotubes as a Potential High-capacity Hydrogen Storage Medium. *Phys. Rev. Lett.* **2005**, *94*, 175501.
(21) Durgun, E.; Ciraci, S.; Yildirim, T. Functionalization of Carbon-based Nanostructures with Light Transition-metal Atoms for Hydrogen Storage. *Phys. Rev. B* **2008**, *77*, 085405.
(22) Shevlin, S. A.; Guo, Z. X. Transition Metal Doping Enhanced Hydrogen Storage in Boron Nitride Systems. *Appl. Phys. Lett.* **2006**, *89*, 153104.
(23) Niemann, M. U.; Srinivasan, S. S.; Phani, A. R.; Kumar, A.; Goswami, D. Y.; Stefanakos, E. K. Nanomaterials for Hydrogen Storage Applications: A Review. *J. Nanomater.* **2008**, *2008*, 950967.
(24) Lavrentiev, V.; Naramoto, H.; Narumi, K.; Sakai, S.; Avramov, P. Planar Doping of Crystalline Fullerene with Cobalt. *Chem. Phys. Lett.* **2006**, *423*, 366−370.
(25) Sakai, S.; Naramoto, H.; Avramov, P. V.; Yaita, T.; Lavrentiev, V.; Narumi, K.; Baba, Y.; Maeda, Y. Comparative Study of Structures and Electrical Properties in Cobalt Fullerene Mixtures by Systematic Change of Cobalt Content. *Thin Solid Films* **2007**, *515*, 7758−7764.
(26) Eldik, R. V.; Cohen, H.; Meyerstein, D. Pressure-Assisted Formation of a Cobalt-Carbon σ Bond: A High-Pressure Pulse Radiolysis Study. *Angew. Chem., Int. Ed.* **1991**, *30*, 1158−1160.
(27) Charlier, J. C.; Iijima, S. Growth Mechanisms of Carbon Nanotubes. *Top. Appl. Phys.* **2001**, *80*, 55−81.
(28) Gao, P.; Wang, Y.; Yang, S. Q.; Chen, Y. J.; Xue, Z.; Wang, L. Q.; Li, G. B.; Sun, Y. Z. Mechanical Alloying Preparation of Fullerene-like Co_3C Nanoparticles with High Hydrogen Storage Ability. *Int. J. Hydrogen Energy* **2012**, *37*, 17126−17130.
(29) Thakur, P.; Kumar, A.; Gautama, S.; Chae, K. H. Electronic Charge Transfer in Cobalt Doped Fullerene Thin Films and Effect of Energetic Ion Impacts by X-ray Absorption Spectroscopy. *Thin Solid Films* **2011**, *519*, 8401−8405.
(30) Du, H. M.; Jiao, L. F.; Wang, Q. H.; Huan, Q. N.; Peng, W. X.; Song, D. W.; Wang, Y. J.; Yuan, H. T. Selenium: Another Metalloid Beneficial for the Electrochemical Performance of Co Electrode in Alkaline Rechargeable Batteries. *J. Power Sources* **2011**, *196*, 10748−10752.
(31) Chung, S. R.; Wang, K. W.; Perng, T. P. Electrochemical Hydrogenation of Crystalline Co Powder. *J. Electrochem. Soc.* **2006**, *153*, A1128−A1131.
(32) Lamari, F. D.; Levesque, D. Hydrogen Adsorption on Functionalized Graphene. *Carbon* **2011**, *49*, 5196−5200.
(33) Sakai, S.; Naramoto, H.; Avramov, P. V.; Yaita, T.; Lavrentiev, V.; Narumi, K.; Baba, Y.; Maeda, Y. Comparative Study of Structures and Electrical Properties in Cobalt-fullerene Mixtures by Systematic Change of Cobalt Content. *Thin Solid Films* **2007**, *515*, 7758−7764.
(34) Porezag, D.; Pederson, R.; Frauenheim, T.; Köhler, T. Structure, Stability, and Vibrational Properties of Polymerized C_{60}. *Phys. Rev, B* **1995**, *52*, 14963−14970.
(35) Plank, W.; Pichler, T.; Kuzmany, H.; Dubay, O.; Tagmatarchis, N.; Prassides, K. Resonance Raman Excitation and Electronic Structure of the Single Bonded Dimers $(C_{60})_2$ and $(C_{59}N)_2$. *Eur. Phys. J. B* **2000**, *17*, 33−42.
(36) Davydov, V. A.; Kashevarova, L. S.; Rakhmanina, A. V.; Senyavin, V. M.; Céolin, R.; Szwarc, H.; Allouchi, H.; Agafonov, V. Spectroscopic Study of Pressure-polymerized Phases of C_{60}. *Phys. Rev. B* **2000**, *61*, 11936−11945.
(37) Hu, D. L.; Pan, B. C.; Li, J. M. Properties of Single-Wall Carbon Nanotubes with Finite Lengths. *Chin. Phys. Lett.* **2001**, *18*, 653−655.
(38) Dillon, A. C.; Jones, K. M.; Bekkedahl, T. A.; Kiang, C. H.; Bethune, D. S.; Heben, M. J. Storage of Hydrogen in Single-walled Carbon Nanotubes. *Nature* **1997**, *386*, 377−379.
(39) Dresselhaus, M. S.; Dresselhaus, G.; Eklund, P. C. *Science of Fullerenes and Carbon Nanotubes*; Academic Press: New York, 1996; p 22.
(40) Lavrentiev, V.; Vacik, J.; Naramoto, H.; Sakai, S. Thermal Effect on Structure Organizations in Cobalt-Fullerene Nanocomposition. *J. Nanosci. Nanotechnol.* **2009**, *9*, 1−6.
(41) Thomsen, E. Niels Stensen-Steno, in the World of Collections and Museums. *Geol. Soc. Am. Mem.* **2009**, *203*, 75−91.
(42) Milchev, A. Electrochemical Phase Formation: Some Fundamental Concepts. *J. Solid State Electro.* **2011**, *15*, 1401−1415.
(43) Biesinger, M. C.; Payne, B. P.; Grosvenor, A. P.; Lau, L. M.; Gerson, A. R.; Smart, R. S. C. Resolving Surface Chemical States in XPS Analysis of First Row Transition Metals, Oxides and Hydroxides: Cr, Mn, Fe, Co and Ni. *Appl. Surf. Sci.* **2011**, *257*, 2717−2730.
(44) Li, X. A.; Han, X. J.; Du, Y. C.; Xu, P. Magnetic and Electromagnetic Properties of Composites of Iron Oxide and Co-B

Alloy Prepared by Chemical Reduction. *J Magn. Magn. Mater.* **2011**, *323*, 14−21.
(45) Enkvist, C.; Lunell, S.; Sjogren, B.; Bruhwiler, P. A.; Svensson, S. The C_{1s} Shakeup Spectra of Buckminsterfullerene, Acenaphthylene, and Naphthalene, Studied by High Resolution X-ray Photoelectron Spectroscopy and Quantum Mechanical Calculations. *J. Chem. Phys.* **1995**, *103*, 6333−6342.
(46) Amelines-Sarria, O.; Dos Santos Claro, P. C.; Schilardi, P. L.; Blum, B.; Rubert, A.; Benitez, G.; Basiuk, V. A.; González Orive, A.; Hernández Creus, A.; Díaz, C.; Salvarezza, R. C. Electronic and Magnetic Properties of C_{60} Thin Films under Ambient Conditions: A Multitechnique Study. *Org. Electron.* **2011**, *12*, 1483−1492.
(47) Ago, H.; Kugler, T.; Cacialli, F.; Salaneck, W. R.; Shaffer, M. S. P.; Windle, A. H.; Friend, R. H. Work Functions and Surface Functional Groups of Multiwall Carbon Nanotubes. *J. Phys. Chem. B* **1999**, *103*, 8116−8121.
(48) Okpalugo, T. I. T.; Papakonstantinou, P.; Murphy, H.; Mclaughlin, J.; Brown, N. M. D. High Resolution XPS Characterization of Chemical Functionalised MWCNTs and SWCNTs. *Carbon* **2005**, *43*, 153−161.
(49) Ho, Y. M.; Liu, J. W.; Qi, J. L.; Zheng, W. T. Spectroscopic Investigation on Carbon Nanotubes Coated with ZnO Nanoparticles. *J. Phys. D: Appl. Phys.* **2008**, *41*, 065308.
(50) Zhang, Y. H.; Jiao, L. F.; Yuan, H. T.; Zhang, Y. Y.; Liu, L.; Wang, Y. J. Effect of Si on Electrochemical Hydrogen Storage Properties of Crystalline Co. *Int. J. Hydrogen Energy* **2008**, *33*, 1317−1322.
(51) Dai, G. P.; Liu, C.; Liu, M.; Wang, M. Z.; Cheng, H. M. Electrochemical Hydrogen Storage Behavior of Ropes of Aligned Single-walled Carbon Nanotubes. *Nano Lett.* **2002**, *2*, 503−506.
(52) Song, D. W.; Wang, Y. J.; Wang, Q. H.; Wang, Y. P.; Jiao, L. F.; Yuan, H. T. Effect and Function Mechanism of Amorphous Sulfur on the Electrochemical Properties of Cobalt Hydroxide Electrode. *J. Power Sources* **2010**, *195*, 7115−7119.
(53) Kuriyama, N.; Sakai, T.; Miyamura, H.; Uehara, I.; Ishikawa, H.; Iwasaki, T. Electrochemical Impedance and Deterioration Behavior of Metal Hydride Electrodes. *J. Alloys Compd.* **1993**, *202*, 183−197.
(54) Liao, B.; Lei, Y. Q.; Chen, L. X.; Lu, G. L.; Pan, H. G.; Wang, Q. D. Effect of the La/Mg Ratio on the Structure and Electrochemical Properties of La_xMg_3-xNi_9 (x=1.6−2.2) Hydrogen Storage Electrode Alloys for Nickel-metal Hydride Batteries. *J. Power Source* **2004**, *129*, 358−367.
(55) Kohno, T.; Yosida, H.; Kawashima; Inaba, T.; Sakai, I.; Yamamoto, M.; Kanda, F. M. Hydrogen Storage Properties of New Ternary System Alloys: La_2MgNi_9, $La_5Mg_2Ni_{23}$, La_3MgNi_{14}. *J. Alloys Compd.* **2000**, *311*, L5−L7.
(56) Song, M. Y.; Ahn, D.; Kwon, I. H.; Chough, S. H. Development of AB_2-type Zr-Ti-Mn-V-Ni-M Hydride Electrode for Ni-MH Secondary Battery. *J. Electrochem. Soc.* **2001**, *148*, A1041−A1044.
(57) Yukawa, H.; Takahashi, Y.; Morinaga, M. Electronic Structures of Hydrogen Storage Compound, TiFe. *Comput. Mater. Sci.* **1999**, *14*, 291−294.
(58) Tian, Q. F.; Zhang, Y.; Sun, L. X.; Xu, F.; Tan, Z. C.; Yuan, H. T. Effects of Pd Substitution on the Electrochemical Properties of $Mg_{0.9}$-$xTi_{0.1}Pd_xNi$ (x=0.04−0.1) Hydrogen Storage Alloys. *J. Power Sources* **2006**, *158*, 1463−1471.
(59) Liu, W.; Lei, Y.; Sun, D.; Wu, J.; Wang, Q. D. A Study of the Degradation of the Electrochemical Capacity of Amorphous $Mg_{50}Ni_{50}$ Alloy. *J. Power Sources* **1996**, *58*, 243−247.
(60) Liu, J. W.; Yuan, H. T.; Cao, J. S.; Wang, Y. J. Effect of Ti-Al Substitution on the Electrochemical Properties of Amorphous MgNi-based Secondary Hydride Electrodes. *J. Alloys Compd.* **2005**, *392*, 300−305.
(61) Wang, Y. D.; Ai, X. P.; Yang, H. X. Effect and Function Mechanism of Amorphous Sulfur on the Electrochemical Properties of Cobalt Hydroxide Electrode. *Chem. Mater.* **2004**, *16*, 5194−5197.
(62) Tan, W. T.; Lim, E. B.; Goh, J. K. Voltammetric Studies of Microcrystalline C_{60} Adhered to a Carbon Electrode Surface and Placed in Contact with Aqueous Electrolyte Containing Potassium Ions. *J. Solid State Electr.* **2005**, *9*, 30−42.
(63) Gao, P.; Yang, S. Q.; Xue, Z.; Liu, G. B.; Zhang, G. L.; Wang, L. Q.; Li, G. B.; Sun, Y. Z.; Chen, Y. J. High Energy Ball-milling Preparation of Co-B Amorphous Alloy with High Electrochemical Hydrogen Storage Ability. *J. Alloys Compd.* **2012**, *539*, 90−96.